

Hierarchical microimaging of bone structure and function

Ralph Müller

Abstract | With recent advances in molecular medicine and disease treatment in osteoporosis, quantitative image processing of three-dimensional bone structures is critical in the context of bone quality assessment. Biomedical imaging technology such as MRI or CT is readily available, but few attempts have been made to expand the capabilities of these systems by integrating quantitative analysis tools and by exploring structure–function relationships in a hierarchical fashion. Nevertheless, such quantitative end points are an important factor for success in basic research and in the development of novel therapeutic strategies. CT is key to these developments, as it images and quantifies bone in three dimensions and provides multiscale biological imaging capabilities with isotropic resolutions of a few millimeters (clinical CT), a few tens of micrometers (microCT) and even as high as 100 nanometers (nanoCT). The technology enables the assessment of the relationship between microstructural and ultrastructural measures of bone quality and certain diseases or therapies. This Review focuses on presenting strategies for three-dimensional approaches to hierarchical biomechanical imaging in the study of microstructural and ultrastructural bone failure. From this Review, it can be concluded that biomechanical imaging is extremely valuable for the study of bone failure mechanisms at different hierarchical levels.

Müller, R. *Nat. Rev. Rheumatol.* 5, 373–381 (2009); doi:10.1038/nrrheum.2009.107

Introduction

Quantitative end points have become an important factor for success in basic research and in the development of novel therapeutic strategies in biology and medicine. Biomedical imaging of three-dimensional (3D) biological structures has, therefore, received increasing attention, for it is often the basis on which both qualitative (that is, visualization) and quantitative (that is, morphometry) images are processed. For the assessment of microstructural tissue properties, in particular, a number of new imaging modalities have been introduced. These techniques can typically be used to visualize a variety of biological materials, including both soft and hard tissues. Whereas soft-tissue imaging is actually a much larger market, with respect to both its demand and commercial availability, and is nowadays regularly used as a standard procedure for imaging biological structures,^{1–5} hard-tissue (that is, bone) imaging has made great progress with respect not only to qualitative imaging but also structural and functional assessment of microstructural images in both human and animal bone.^{6–15}

Bone is one of the most frequently investigated biological materials, owing to its primary function of providing skeletal stability. Bone is susceptible to different local stimuli, including mechanical forces, and has great capabilities to adapt its mechanical properties to environmental changes. Nevertheless, aging or hormonal changes can lead bone to lose this capacity to remodel

appropriately, resulting in loss of strength and increased fracture risk. With the emergence of accurate and precise bone densitometry over the last two decades, bone mass has become a primary end point in the diagnosis and monitoring of osteoporosis. Strong correlations between bone mass and the mechanical properties of trabecular bone have been demonstrated in large populations.^{16–22} However, changes in mass can explain only part of the variation in trabecular bone strength between individuals, leaving up to 90% unexplained.²³ Thus, the accurate assessment of bone fracture risk in a clinical environment solely on the basis of bone densitometry is difficult to achieve. With so much variation unexplained by bone mass changes, other factors, such as bone microarchitecture, bone cell distribution, bone remodeling, the distribution of microcracks or microdamage and the properties of bone matrix material, must also have important roles. Although attention in recent years has been focused on the mechanical analysis of trabecular bone, it is necessary to understand that the fracture behavior of cortical bone is also very important and cannot be neglected for accurate prediction of fracture risk in whole bones.²⁴ The factors discussed above, together with bone mineral density, are often collectively referred to as ‘bone quality’.^{25–27} However, the relative contribution of each of these different factors to the overall mechanical competence of bone is still poorly understood.

The ‘gold standard’ method for determining bone competence is mechanical testing. Classic mechanical testing²⁸ provides detailed information on whole-bone mechanical

Institute for Biomechanics, Department of Mechanical and Process Engineering, ETH Zürich, Zürich, Switzerland.

Correspondence: Institute for Biomechanics, Department of Mechanical and Process Engineering, ETH Zürich, Wolfgang-Pauli-Strasse 10, 8093 Zürich, Switzerland
ram@ethz.ch

Competing interests

The author declares no competing interests.

Key points

- Over the last decade, microCT has been established as a quantitative microscope, especially for the assessment of hard tissues
- MicroCT is fast, reliable and yields accurate and precise morphometric indices that are used for the diagnosis of disease and the monitoring of treatment regimens in both preclinical and clinical research
- Biomechanical imaging (i.e. the combination of time-lapsed microCT imaging and concomitant mechanical testing) enables the study of bone failure initiation and propagation in a hierarchical fashion
- Synchrotron radiation and advanced desktop nanoCT systems facilitate exploring the bone ultrastructure with submicrometer resolutions, enabling static quantitative morphometry of cortical bone canals and cell lacunae as well as biomechanical imaging of microcrack initiation and propagation

and bone matrix material properties, but does not reveal local failure properties. Bone failure is a time-dependent, nonlinear event that involves high local deformations and local fractures that build up to macroscopic failure in the final stage.²⁹ Although some work has been done to clarify the characteristics of bone failure, basic knowledge of how failure originates within both trabecular and cortical bone is still lacking. However, to estimate an individual patient's risk of fracture, an extended understanding of the failure behavior of trabecular and cortical bone is essential. For this reason, imaging techniques that enable the study of bone tissue in a nondestructive and time-lapsed fashion *in situ* are very important. The incorporation of such biomechanical or functional imaging methods with mechanical testing will provide insight into bone deformation and failure characteristics at various levels of structural organization.

Hierarchical imaging of microarchitecture

Hierarchical imaging is the ability to resolve anatomical features at various resolutions and size scales using essentially the same imaging modality, and ideally covering a few orders of magnitude in resolution. This ability would enable the measurement of features at resolutions from organ level (500 μm) to structural level (50 μm), tissue level (5 μm), and even cellular level (0.5 μm) using the same technology.

CT is such an approach to imaging and quantifying both trabecular and cortical bone in 3D: it provides multiscale biological imaging with isotropic resolutions ranging from a few millimeters (clinical CT), to a few tens of micrometers (microCT), down to 100 nanometers (nanoCT) (Figure 1). The application of lower-resolution imaging technologies in clinical practice have been reviewed extensively in the last few years,^{9,12,14,15,30,31} whereas very few reviews exist of high-resolution microCT and nanoCT; this Review, therefore, focuses on these technologies.

Early implementations of 3D microCT focused on methodological aspects, and required equipment that was not widely available;³² a more recent development has emphasized the practical aspects of microCT imaging.³³ This and other similar commercially-available

systems can be routinely used in basic research and clinical laboratories. Also referred to as 'desktop microCT', they provide nominal resolutions in the approximate range of 5–100 μm , and can measure specimens with diameters of a few millimeters to 100 mm. Desktop microCT is a precise and validated imaging technique,^{34–40} and has been used extensively in the assessment of micro-architectural bone (Figure 2) in the context of investigating different diseases and their treatment, such as osteoporosis^{41–49} and osteoarthritis;^{50–53} genetics and gene therapy,^{54–57} dental research and implants,^{58–61} tissue engineering and biomaterials,^{13,62–66} and the validation of other techniques aimed at investigating bone microstructure in a more clinical setting.^{67–69} This list is by no means complete: more than 1,800 papers on microCT imaging of bone had been published by April 2009. Thus, the ISI citation index was often considered to select those articles best representing the use of microCT in the different fields discussed. This was done on the assumption that highly cited articles represent the most important contributions in their respective fields.

Since the introduction of these systems, there has been an increasing demand for microCT technology throughout the world. With the advent of third-generation synchrotron radiation facilities, microCT with resolutions of 1 μm and higher (termed 'nanoCT') became feasible.^{70–72} Synchrotron radiation has several advantages over conventional X-rays, including a high brilliance, which allows higher resolutions in nanoCT applications,⁷³ and the use of a monochromatic beam that produces accurate density representations.^{74,75} The high resolution of synchrotron radiation microCT and nanoCT systems enables an even higher level of magnification, which in bone research is necessary to investigate 3D properties of ultrastructural features, such as the canal network,^{76,77} osteocyte lacunae⁷⁸ (Figure 3) and even single cells,⁷⁹ as well as direct functional outcomes, such as microcracks and microfractures.^{80–82}

Quantification of microarchitecture

A method of quantitatively describing bone architecture and the changes associated with age or disease stage is the calculation of morphometric indices, also referred to as quantitative bone morphometry. In the past, structural properties of trabecular bone were investigated by the examination of two-dimensional (2D) sections of bone biopsies; 3D morphometric parameters were then derived from 2D images using stereological methods.⁸³ The correlations between 2D histology and 3D microCT are highly significant for bone volume density and bone surface density,³⁶ which can be directly obtained from both 2D and 3D images; by contrast, a range of important parameters, such as trabecular thickness, trabecular separation and trabecular number have to be derived indirectly from 2D images by assuming a fixed-structure model. Typically, an 'ideal plate' or 'ideal rod' model is used, meaning trabecular bone consisting solely of either plates or rods; however, such assumptions are critical to

the accuracy of the measurements, owing to the fact that trabecular bone architecture differs by site and that it continuously changes its structure as a result of remodeling. This variability was demonstrated a decade ago in a large study of 260 human bone biopsies taken from five different skeletal sites, which were evaluated with both traditional 2D histomorphometry and newly developed 3D methods.⁸⁴ For trabecular thickness, trabecular separation and trabecular number, the two methods produced markedly different results, and correlations between parameters calculated either from 2D or 3D images were only moderate. Furthermore, the strength of the correlations depended on anatomical site, owing to anatomical differences in bone architecture: the discrepancy between the true trabecular architecture and the assumed structure is larger for one site than for another. For this reason, deviation from the assumed model will lead to an unpredictable error in indirectly derived parameters. This is particularly true in studies that follow changes in bone structure over the course of age-related bone loss, and in those that evaluate drug therapy. In such cases, a predefined model assumption could easily overestimate or underestimate the effects of bone atrophy depending on the index assessed.

For these reasons, and in order to take full advantage of volumetric measurements, several 3D image-processing methods have been developed that enable direct quantification of bone microarchitecture.^{84,85} These techniques calculate actual distances in 3D space and, therefore, do not rely on an assumed model type and are not biased by possible deviations. In addition to the computation of direct metric parameters, non-metric parameters can be calculated to describe the 3D nature of a bone structure (Box 1). An estimation of how plate-like or rod-like a bone structure is can be achieved using the structure model index.⁸⁶ Another parameter often used as an architectural index is structural anisotropy,⁸⁷ a measure of the primary orientation of the trabeculae (often referred to as degree of anisotropy). The connectivity density index was introduced to characterize the number of possible paths that connect the analyzed bone structure from one end to the other, expressed as the number of connections per mm^3 .⁸⁸

Quantitative assessment of 3D trabecular bone morphology applies to porous structures as a whole and not to their individual elements. Although such studies demonstrate the importance of architectural bone properties in a statistical sense, they do not explain how the microarchitecture physically contributes to the mechanical failure behavior of bone. The capacity to assess this is actually one of the biggest advantages of 3D image analysis, as it enables topological analysis that targets individual elements rather than the structure as a whole. The mathematical background to digital topological analysis has been developed by Serra,⁸⁹ and has since been adapted for applications in bone.⁹⁰ Using this method, the structural properties of individual trabecular elements can be calculated using volumetric spatial decomposition.⁹¹ The

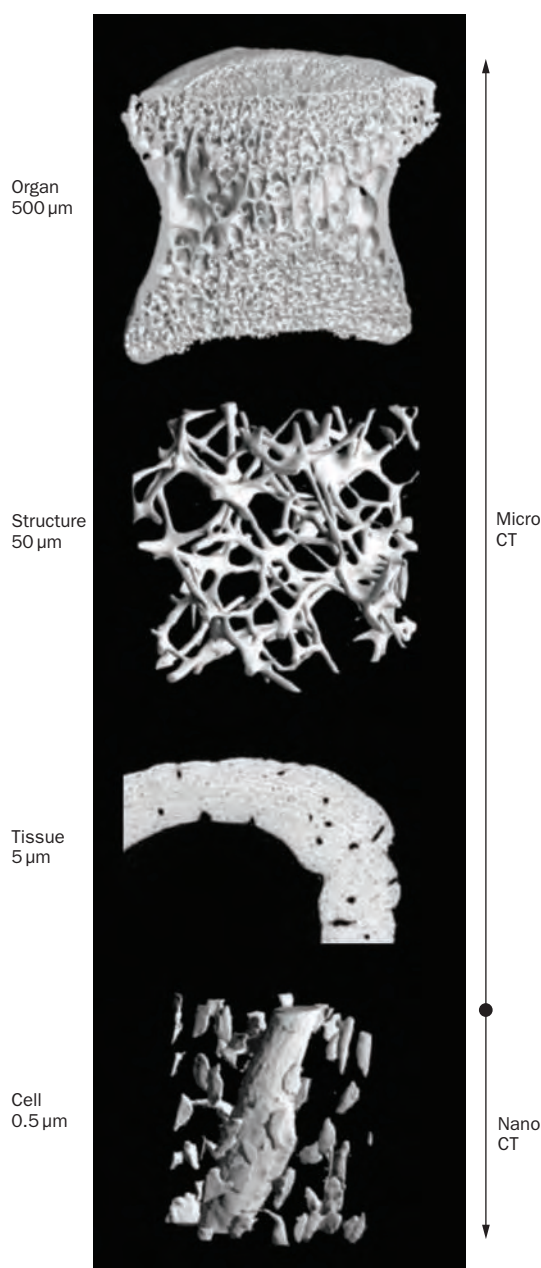


Figure 1 | Schematic overview of hierarchical imaging with microCT and nanoCT. At the organ level, an image of a cut-through vertebral body, obtained using desktop microCT, demonstrates the extensive heterogeneity in the vertebra of a macaque. At the structural level, desktop microCT illustrates the three-dimensional trabecular microarchitecture in a human vertebral sample. At the tissue level, synchrotron radiation microCT of a cortical bone sample from a mouse femur illustrates vascular channels (large holes) and cell lacunae (small holes). Synchrotron radiation microCT at the cellular level shows osteocytic lacunae arranged around a microvessel in mouse cortical bone. Permission obtained from Springer Ltd © Müller, R. *et al.* Functional microimaging at the interface of bone mechanics and biology. In *Mechanics of Biological Tissue, Part V* (Eds Holzapfel, G. & Odgen, R. W.) 473–487 (Springer, Heidelberg, 2006).

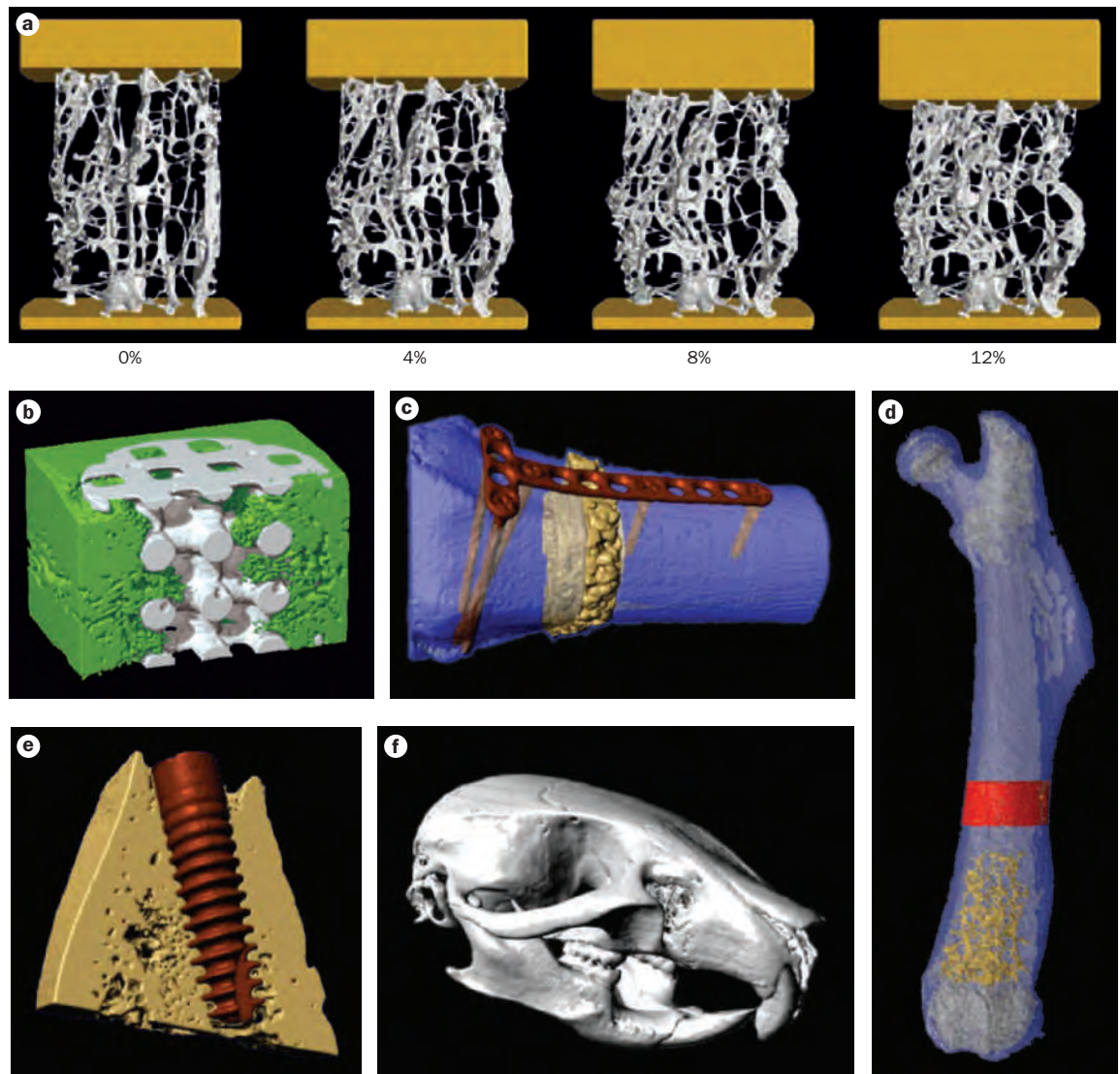


Figure 2 | Typical applications of microCT in the imaging of bone. **a** | Human spine trabecular bone structure in a two-plate compression testing experiment. **b** | Three-dimensional reconstruction of scaffold (grey) and bone ingrowth (green) in a minipig model of bone regeneration. Only part of the cylindrical scaffold is displayed, to enable a view of the inside of the scaffold. **c** | Performance analysis of a bone replacement material in a sheep fracture repair model. A gap was cut in the long bone (grey) and filled with bone replacement material (yellow); the fracture was fixed using a conventional T-plate. **d** | Mouse femur. Typically in bone research, different compartments (grey, full bone; red, cortical ring; yellow, trabecular region) are selected to compute morphometric indices. **e** | Titanium screw (red) in rat bone (yellow). **f** | Mouse cranium. Permission obtained from Springer Ltd © Stauber, M. & Müller, R. *Methods Mol. Biol.* **455**, 273–292 (2008).

ability to spatially break down the bone microarchitecture and extract information about individual structural elements (for example, trabecular rods and plates) enables local bone morphometry; that is, the shape and form of each single bone element can be individually determined.⁹¹ With this method it is possible to perform more-detailed analyses of 3D structures and to analyze the individual contribution of rods and plates to bone aging⁹² and to the mechanical competence of trabecular bone.⁹³ As an example, in a study of human vertebral bone samples, a multiple linear regression model combining mean trabecular separation, mean slenderness of the rods, and

the relative amount of rod volume to total bone volume was able to explain 90% of the variance in bone stiffness. This model could not be improved by adding bone volume density as an independent variable.⁹⁴

Quantitative morphometry has also been applied to the 3D analysis of cortical bone ultrastructure,^{76,77} as there is a growing body of work implicating cortical bone as an important target for bone quality assessment and pharmacological treatment. At the tissue level, the intricate canal network in cortical bone can be not only visualized (Figure 3), but also analyzed with respect to the length and size of each canal as well as to topology.⁹⁵

At the cellular level, negative imaging⁷⁸ of the mineralized phase provides 3D imprints of osteocyte lacunae, which can be analyzed with respect to cell number and shape. The influence of these novel ultrastructural cortical bone properties have been shown to influence the mechanical behavior of whole bones.⁹⁶

Additionally, CT allows quantification of not only bone microstructure and ultrastructure but also bone mineralization, especially in cortical bone,⁷⁴ but in trabecular bone as well.⁷⁵ This is important, as bone mineralization is estimated to disproportionately contribute to bone strength⁹⁷ and is believed to have a major role in explaining the antifracture efficacy of bisphosphonate treatment.^{98,99} Although monochromatic beams assess mineralization very accurately, the same accuracy cannot be determined by the use of polychromatic X-ray sources,^{100,101} which can sometimes even lead to large errors in the determination of tissue mineralization.¹⁰² This issue clearly demands further investigation before these systems can be fully trusted to analyze the degree of mineralization both on the organ and tissue levels.

Image-guided assessment of competence

Although the inclusion of ultrastructural bone properties has strongly improved the prediction of bone competence,^{103,104} they only do so in a statistical sense. As mentioned earlier, these properties do not explain the real physical contribution of the microarchitecture to the mechanical failure behavior of bone. To understand in more detail how differences in bone architecture influence bone competence, insight into load transfer through the bone is needed. With the advent of fast and powerful computers, simulation techniques such as micro-finite element modeling are becoming popular for investigating the mechanical properties of bone. Nevertheless, micro-finite element models have thus far mainly assessed bone loading in the elastic range, on the basis of the notion that the strength of bone is highly correlated with its elastic properties.^{105,106} However, bone fracture is a time-dependent, nonlinear event that involves local material failure. Although some failure characteristics have been elucidated, basic knowledge of local bone failure is still lacking. Parameters estimated or computed from images accurately predict mechanical properties for linear behavior (for example, stiffness, modulus) and to some extent ultimate behavior (for example, maximal strength). However, image-based approaches to determining mechanical properties beyond yield such as toughness, ductility and brittleness are difficult to perform; furthermore, most mechanical testing focuses on linear-elastic behavior. Nevertheless, in estimating the risk of spontaneous fractures, an extended understanding of the nonlinear failure behavior of both cortical and trabecular bone is essential.

Image-guided failure assessment (IGFA)^{107,108} provides insight into failure behavior by enabling direct, time-lapsed, 3D visualization and quantification of fracture progression on the microscopic level. Additionally, a

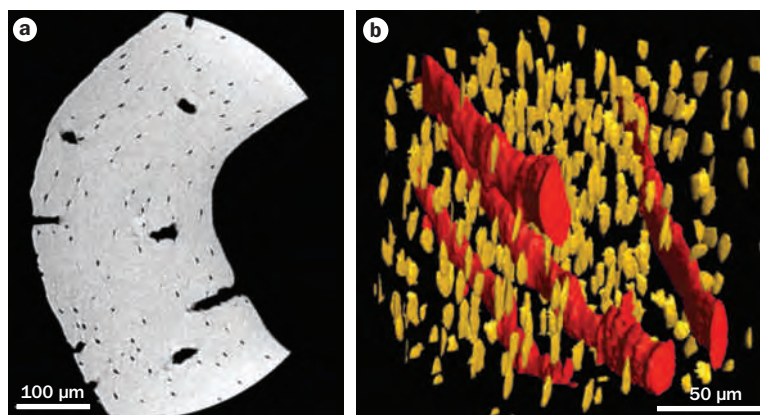


Figure 3 | Ultrastructural representation of void spaces within cortical bone of a mouse femur. **a** | Two-dimensional nanoCT slice of the cortical mid-diaphysis in transverse view, showing sections through canals and osteocyte lacunae. Data was assessed at the Swiss Light Source at 700 nm nominal resolution. **b** | Three-dimensional representation of the cortical subvolume, visualizing the extent of the canal network (red) and osteocyte lacunae (yellow). Volumetric information was extracted from the same data using negative imaging. Reproduced from Schneider, P *et al.* *J. Bone Miner. Res.* **22**, 1557–1570 (2007), with permission from the American Society for Bone and Mineral Research.

Box 1 | Measures of bone structure in three dimensions as assessed by CT

Metric parameters

Bone volume density: relative volume of mineralized tissue per total volume

Bone surface density: relative volume of bone surface per total volume

Trabecular thickness: average thickness of the individual plates and rods in the structure

Trabecular separation: thickness of the spaces between trabeculae

Trabecular number: number of trabeculae per unit length

Non-metric parameters

Structure model index: estimates ratio of plates and rod composing the structure

Structural anisotropy: a measure of the primary orientation of the trabeculae (also referred to as degree of anisotropy)

Connectivity density: characterizes the number of possible paths that connect the analyzed bone structure from one end to the other

number of image analysis methods have been developed to identify and classify individual rods and plates, to then track those elements over the time course of failure, and to eventually compute local displacements and strains at each consecutive compression step.¹⁰⁹ The results of time-lapsed compression tests showed that average strains were much smaller than the externally applied strain, but that maximum local strain values were five to eight times greater than the externally applied strain, providing further evidence for a band-like, local failure behavior of trabecular bone (Figure 2a).¹⁰⁹

Another study combined histological damage labeling, microCT and image-based finite element analysis to detect regions of compression microdamage in bovine tibial trabecular bone.¹¹⁰ The pattern of trabecular failure

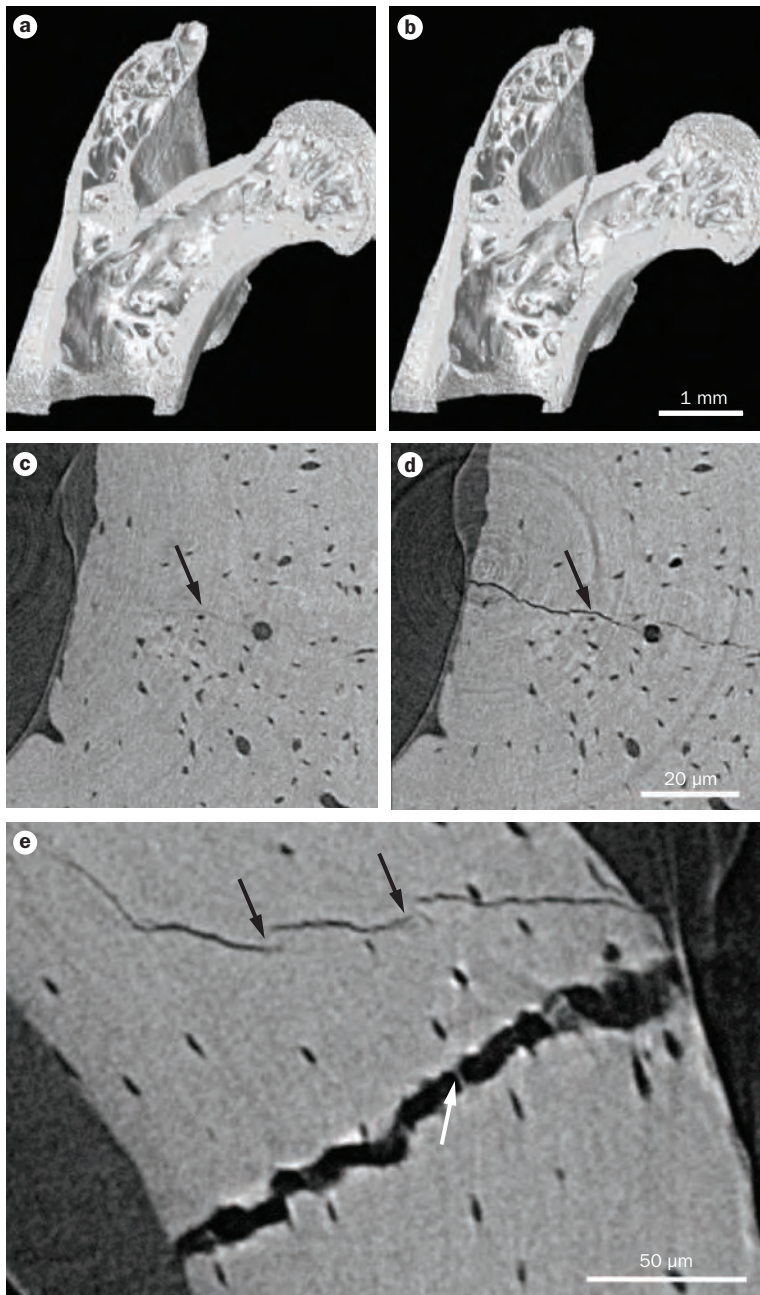


Figure 4 | Hierarchical imaging of bone function with synchrotron radiation CT. Image-guided failure assessment illustrates compression and fracture at a proximal mouse femur **a** | in the uncompressed femoral neck, and **b** | after displacement of the femoral neck. Nominal resolution 3.5 μm for both images. **c** | Reconstructed slices of mouse femoral bone from the cortical mid-diaphysis. Nominal resolution 700 nm; 1% apparent strain. A microcrack is faintly visible (black arrow). **d** | At 2% apparent strain, the microcrack has propagated and is now clearly visible (black arrow). Nominal resolution 700 nm. **e** | Cortical bone at 1% strain with a microcrack and a microfracture. Uncracked ligament bridges intersect the microcrack (black arrows) and span the microfracture (white arrow). Nominal resolution 700 nm.

observed with microCT positively correlated with the polarity and distribution of stresses within an individual trabecula as predicted by finite element analysis. Furthermore, a comparison of individual trabeculae

revealed that local stresses and strains were significantly higher in damaged trabeculae than in undamaged trabeculae.¹¹⁰ More recently, IGFA has been expanded to investigate the failure behavior of whole vertebral bodies,¹¹¹ by use of a non-contact method that enables *in vitro* quantification of endplate deformation under axial load in intact human cadaver specimens. The major advantage of this method is the ability to perform a repeated-measures experimental design, which enables the assessment of endplate deformation using time-lapsed microCT imaging in the same sample with increasing load. The approach can be used to analyze intact functional spine units and even instrumented specimens.¹¹¹

Whereas desktop microCT studies focus mostly on the microstructural level, synchrotron radiation microCT and nanoCT enable analysis of the next level of hierarchy. With the advent of these synchrotron radiation techniques, bone failure can be investigated on the micrometer and even the submicrometer level by direct observation of microcracks and microfractures in a fully nondestructive and even in a time-lapsed fashion. The development of an *in situ* mechanical compression device capable of exerting both static and dynamic displacements on experimental samples has also improved the investigation of different failure mechanisms at the microstructural level.⁸⁰ Applied in a study of failure mechanisms in trabecular bone, these methods revealed differences in the initiation and propagation of failure between fatigued and nonfatigued bovine bone samples. As expected, the nonfatigued sample exhibited a distinct band of localized failure, whereas the fatigued sample failed in a burst-like fashion. Almost all of the microscopic cracks observed in both fatigued and nonfatigued samples were connected to a clearly recognizable bone surface. This also means that microcracks typically will not develop solely within the bone matrix but will always initiate or at least extend to the bone surface. Thus, 3D methods to detect and analyze microcracks are preferred over 2D methods, where the orientation of the cut plane can introduce artifacts in the interpretation of the microcracks as being linear or fully inside the bone matrix. Further investigation revealed that trabecular bone often fails through the delamination of mineralized collagen fibrils¹¹²—the basic building blocks of bone matrix at the supramolecular level¹¹³—thereby providing a mechanism for energy dissipation while conserving trabecular bone architecture. Microcracking, then, is of major importance in the determination of bone failure behavior in the post-yield phase (that is, toughness).

The concept of hierarchical biomechanical imaging has also been used to investigate the failure behavior of cortical bone. For instance, compression testing performed concurrently with synchrotron radiation CT has been used to observe, in 3D, fracture initiation and propagation in mouse femur.¹¹⁴ During compression of the femoral head, synchrotron radiation CT showed that bone failed at the location where tensile stresses were highest in the cortical bone (that is, the superior femoral neck; Figure 4a

and 4b). In addition, uncracked ligament bridges were imaged for the first time in 3D at a nominal resolution of 700 nm,¹¹⁴ displaying the relationship of microcracks not only to the canal network but also to the much smaller osteocyte lacunae (Figure 4c and 4d). The results showed that osteocyte lacunae do not contribute to the initiation of cracks, but are important in their propagation. Of note, many cracks initiated at the open surfaces of the canal network, a mechanism that was recently shown to have an important role in human cortical bone failure.⁸² Uncracked ligament bridging in bone was first reported as a toughening mechanism¹¹⁵ that involves 2D uncracked regions along the crack path which, in the first phase of bone fracture, can bridge the crack on opening. At that point of bone failure, the long axes of the uncracked-ligament bridges are mostly aligned parallel to the direction of crack propagation or to the long axis of the crack (Figure 4e). Nevertheless, one has to bear in mind that rodent bone does not give reliable information about human bone in all cases and, therefore, care should be taken in the extrapolation of experimental data to clinical situations. The development of high-speed imaging that produces full tomographs at microscopic resolution in only a few seconds¹¹⁶ will facilitate high-throughput biomechanical imaging and, therefore, also enable imaging of dynamic failure behavior.¹¹⁷

Clinical translation

As discussed in this Review, the mechanical properties of bone depend on bone density, microstructure and ultrastructure. For the clinician, however, the prediction of bone quality in individual patients is essentially restricted to the quantitative analysis of bone density alone. By use of hierarchical bone imaging, it is possible, for the first time, to assess the density and the trabecular and cortical macrostructure, microstructure and ultrastructure of bones using fully nondestructive measurement techniques. Whether these sophisticated engineering approaches will find their way from research to the clinic is yet to be determined, but it seems clear that there is great potential in the clinical arena for noninvasive hierarchical imaging. Whereas high-resolution *in vivo* imaging at the microstructural level is already possible and prospects for improved clinical and diagnostic purposes have been demonstrated,^{15,31}

measurements of ultrastructural bone features, such as microcracks or the shape and distribution of osteocyte lacunae, are still limited to the analysis of excised bone biopsies. Nevertheless, paired iliac crest bone biopsy has been and still is being used to determine responses to treatment,^{46,49,75} and is therefore still an important tool in clinical practice. Clearly, however, this tool is far from ideal for several reasons. First, the procedure requires taking two invasive biopsies, which can be problematic; second, the biopsy specimens are necessarily small; and third, two different bone architectures are being evaluated.

Conclusions

Microarchitectural bone imaging is a nondestructive, noninvasive and precise procedure that enables the measurement of trabecular and cortical bone as well as the repetitive assessment and computation of 3D microstructural and micromechanical properties. The procedure can help improve predictions of fracture risk, clarify the pathophysiology of skeletal diseases, and define the response to therapy.

Biomechanical or functional imaging of bone, comprising the combination of biomechanical testing and time-lapsed imaging, is extremely valuable in studying bone failure mechanisms and how bone structure influences its functional behavior. Hierarchical investigations of microcrack initiation and propagation using synchrotron light and other high-resolution imaging techniques will lead to a better understanding of the relative contribution of the different hierarchical levels to the overall competence of bone.

Review criteria

ISI and PubMed databases were searched for published original articles that were related to the microtomographic imaging of bone. Search terms included "bone" in combination with "micro computed tomography", "mu CT" and "micro CT". Manuscripts reviewed were full-text and published in English. The citations from these articles were also used to identify additional manuscripts of interest. The ISI citation index was used to identify highly cited articles in the field. No restrictions were placed on the publication date. The reference list was last updated in April 2009.

- Paulus, M. J., Gleason, S. S., Easterly, M. E. & Foltz, C. J. A review of high-resolution X-ray computed tomography and other imaging modalities for small animal research. *Lab Anim. (NY)* **30**, 36–45 (2001).
- Ritman, E. L. Micro-computed tomography—current status and developments. *Annu. Rev. Biomed. Eng.* **6**, 185–208 (2004).
- Badea, C. T., Fubara, B., Hedlund, L. W. & Johnson, G. A. 4-D micro-CT of the mouse heart. *Mol. Imaging* **4**, 110–116 (2005).
- Heinzer, S. *et al.* Hierarchical microimaging for multiscale analysis of large vascular networks. *Neuroimage* **32**, 626–636 (2006).
- Bullitt, E., Reardon, D. A. & Smith, J. K. A review of micro- and macrovascular analyses in the assessment of tumor-associated vasculature as visualized by MR. *Neuroimage* **37** (Suppl. 1), S116–S119 (2007).
- Goldstein, S. A., Goulet, R. W. & McCubbrey, D. Measurement and significance of three-dimensional architecture to the mechanical integrity of trabecular bone. *Calcif. Tissue Int.* **53** (Suppl. 1), S127–S132 (1993).
- Müller, R. & Rügsegger, P. Micro-tomographic imaging for the nondestructive evaluation of trabecular bone architecture. *Stud. Health Technol. Inform.* **40**, 61–79 (1997).
- Ito, M. *et al.* Analysis of trabecular microarchitecture of human iliac bone using microcomputed tomography in patients with hip arthrosis with or without vertebral fracture. *Bone* **23**, 163–169 (1998).
- Genant, H. K. *et al.* Advanced imaging of bone macro and micro structure. *Bone* **25**, 149–152 (1999).
- McCreadie, B. R., Goulet, R. W., Feldkamp, L. A. & Goldstein, S. A., Hierarchical structure of bone and micro-computed tomography. *Adv. Exp. Med. Biol.* **496**, 67–83 (2001).
- Müller, R. The Zürich experience: one decade of three-dimensional high-resolution computed tomography. *Top. Magn. Reson. Imaging* **13**, 307–322 (2002).
- Link, T. M. & Majumdar, S. Current diagnostic techniques in the evaluation of bone architecture. *Curr. Osteoporos. Rep.* **2**, 47–52 (2004).

13. Porter, B., Zauel, R., Stockman, H., Guldberg, R. & Fyhrie, D. 3-D computational modeling of media flow through scaffolds in a perfusion bioreactor. *J. Biomech.* **38**, 543–549 (2005).
14. Wehrli, F. W. Structural and functional assessment of trabecular and cortical bone by micro magnetic resonance imaging. *J. Magn. Reson. Imaging* **25**, 390–409 (2007).
15. Bouxsein, M. L. Technology insight: noninvasive assessment of bone strength in osteoporosis. *Nat. Clin. Pract. Rheumatol.* **4**, 310–318 (2008).
16. McElhaney, J. H. et al. Mechanical properties of cranial bone. *J. Biomech.* **3**, 495 (1970).
17. Carter, D. R. & Hayes, W. C. The compressive behavior of bone as a two-phase porous structure. *J. Bone Joint Surg. Am.* **59**, 954–962 (1977).
18. Williams, J. L. & Lewis, J. L. Properties and an anisotropic model of cancellous bone from the proximal tibial epiphysis. *J. Biomech. Eng.* **104**, 50–56 (1982).
19. Rice, J. C., Cowin, S. C. & Bowman, J. A. On the dependence of the elasticity and strength of cancellous bone on apparent density. *J. Biomech.* **21**, 155–168 (1988).
20. Odgaard, A. & Linde, F. The underestimation of Young's modulus in compressive testing of cancellous bone specimens. *J. Biomech.* **24**, 691–698 (1991).
21. Keller, T. S. Predicting the compressive mechanical behavior of bone. *J. Biomech.* **27**, 1159–1168 (1994).
22. Keaveny, T. M., Guo, X. E., Wachtel, E. F., McMahon, T. A. & Hayes, W. C. Trabecular bone exhibits fully linear elastic behavior and yields at low strains. *J. Biomech.* **27**, 1127–1136 (1994).
23. Ciarelli, M. J., Goldstein, S. A., Kuhn, J. L., Cody, D. D. & Brown, M. B. Evaluation of orthogonal mechanical properties and density of human trabecular bone from the major metaphyseal regions with materials testing and computed tomography. *J. Orthop. Res.* **9**, 674–682 (1991).
24. Augat, P. & Schorlemmer, S. The role of cortical bone and its microstructure in bone strength. *Age Ageing* **35** (Suppl. 2), ii27–ii31 (2006).
25. Bouxsein, M. L. Bone quality: where do we go from here? *Osteoporos. Int.* **14** (Suppl. 5), S118–S127 (2003).
26. Felsenberg, D. & Boonen, S. The bone quality framework: determinants of bone strength and their interrelationships and implications for osteoporosis management. *Clin. Ther.* **27**, 1–11 (2005).
27. Seeman, E. & Delmas, P. D. Bone quality—the material and structural basis of bone strength and fragility. *N. Engl. J. Med.* **354**, 2250–2261 (2006).
28. Turner, C. H. & Burr, D. B. Basic biomechanical measurements of bone: a tutorial. *Bone* **14**, 595–608 (1993).
29. Bay, B. K., Yerby, S. A., McLain, R. F. & Toh, E. Measurement of strain distributions within vertebral body sections by texture correlation. *Spine* **24**, 10–17 (1999).
30. Majumdar, S. Current technologies in the evaluation of bone architecture. *Curr. Osteoporos. Rep.* **1**, 105–109 (2003).
31. van Lenthe, G. H. & Müller, R. CT-based visualization and quantification of bone microstructure *in vivo*. *Bonekey Osteovision* **5**, 410–425 (2008).
32. Feldkamp, L. A., Goldstein, S. A., Parfitt, A. M., Jesion, G. & Kleerekoper, M. The direct examination of three-dimensional bone architecture *in vitro* by computed tomography. *J. Bone Miner. Res.* **4**, 3–11 (1989).
33. Rüeggsegger, P., Koller, B. & Müller, R. A microtomographic system for the nondestructive evaluation of bone architecture. *Calcif. Tissue Int.* **58**, 24–29 (1996).
34. Kuhn, J. L., Goldstein, S. A., Feldkamp, L. A., Goulet, R. W. & Jesion, G. Evaluation of a microcomputed tomography system to study trabecular bone structure. *J. Orthop. Res.* **8**, 833–842 (1990).
35. Uchiyama, T. et al. A morphometric comparison of trabecular structure of human ilium between microcomputed tomography and conventional histomorphometry. *Calcif. Tissue Int.* **61**, 493–498 (1997).
36. Müller, R. et al. Morphometric analysis of human bone biopsies: a quantitative structural comparison of histological sections and microcomputed tomography. *Bone* **23**, 59–66 (1998).
37. Graichen, H. et al. A non-destructive technique for 3-D microstructural phenotypic characterisation of bones in genetically altered mice: preliminary data in growth hormone transgenic animals and normal controls. *Anat. Embryol. (Berl.)* **199**, 239–248 (1998).
38. Kapadia, R. D. et al. Applications of micro-CT and MR microscopy to study pre-clinical models of osteoporosis and osteoarthritis. *Technol. Health Care* **6**, 361–372 (1998).
39. Balto, K., Müller, R., Carrington, D. C., Dobeck, J. & Stashenko, P. Quantification of periapical bone destruction in mice by micro-computed tomography. *J. Dent. Res.* **79**, 35–40 (2000).
40. Yamashita, T., Nabeshima, Y. & Noda, M. High-resolution micro-computed tomography analyses of the abnormal trabecular bone structures in klotho gene mutant mice. *J. Endocrinol.* **164**, 239–245 (2000).
41. Goulet, R. W. et al. The relationship between the structural and orthogonal compressive properties of trabecular bone. *J. Biomech.* **27**, 375–389 (1994).
42. Ulrich, D., van Rietbergen, B., Laib, A. & Rueggsegger, P. The ability of three-dimensional structural indices to reflect mechanical aspects of trabecular bone. *Bone* **25**, 55–60 (1999).
43. Yoshitake, H., Rittling, S. R., Denhardt, D. T. & Noda, M. Osteopontin-deficient mice are resistant to ovariectomy-induced bone resorption. *Proc. Natl Acad. Sci USA* **96**, 8156–8160 (1999).
44. Ding, M. & Hvid, I. Quantification of age-related changes in the structure model type and trabecular thickness of human tibial cancellous bone. *Bone* **26**, 291–295 (2000).
45. Alexander, J. M. et al. Human parathyroid hormone 1–34 reverses bone loss in ovariectomized mice. *J. Bone Miner. Res.* **16**, 1665–1673 (2001).
46. Dempster, D. W. et al. Effects of daily treatment with parathyroid hormone on bone microarchitecture and turnover in patients with osteoporosis: a paired biopsy study. *J. Bone Miner. Res.* **16**, 1846–1853 (2001).
47. Borah, B. et al. Risedronate preserves trabecular architecture and increases bone strength in vertebrae of ovariectomized minipigs as measured by three-dimensional microcomputed tomography. *J. Bone Miner. Res.* **17**, 1139–1147 (2002).
48. Babij, P. et al. High bone mass in mice expressing a mutant LRP5 gene. *J. Bone Miner. Res.* **18**, 960–974 (2003).
49. Borah, B. et al. Risedronate preserves bone architecture in postmenopausal women with osteoporosis as measured by three-dimensional microcomputed tomography. *Bone* **34**, 736–746 (2004).
50. Dedrick, D. K. et al. A longitudinal study of subchondral plate and trabecular bone in cruciate-deficient dogs with osteoarthritis followed up for 54 months. *Arthritis Rheum.* **36**, 1460–1467 (1993).
51. Badger, A. M. et al. Disease-modifying activity of SB 242235, a selective inhibitor of p38 mitogen-activated protein kinase, in rat adjuvant-induced arthritis. *Arthritis Rheum.* **43**, 175–183 (2000).
52. Pettit, A. R. et al. TRANCE/RANKL knockout mice are protected from bone erosion in a serum transfer model of arthritis. *Am. J. Pathol.* **159**, 1689–1699 (2001).
53. Day, J. S. et al. A decreased subchondral trabecular bone tissue elastic modulus is associated with pre-arthritis cartilage damage. *J. Orthop. Res.* **19**, 914–918 (2001).
54. Turner, C. H. et al. Genetic regulation of cortical and trabecular bone strength and microstructure in inbred strains of mice. *J. Bone Miner. Res.* **15**, 1126–1131 (2000).
55. Moutsatsos, I. K. et al. Exogenously regulated stem cell-mediated gene therapy for bone regeneration. *Mol. Ther.* **3**, 449–461 (2001).
56. Bouxsein, M. L. et al. Mapping quantitative trait loci for vertebral trabecular bone volume fraction and microarchitecture in mice. *J. Bone Miner. Res.* **19**, 587–599 (2004).
57. Huang, Y. C., Simmons, C., Kaigler, D., Rice, K. G. & Mooney, D. J. Bone regeneration in a rat cranial defect with delivery of PEI-condensed plasmid DNA encoding for bone morphogenetic protein-4 (BMP-4). *Gene Ther.* **12**, 418–426 (2005).
58. Giesen, E. B. & van Eijden, T. M. The three-dimensional cancellous bone architecture of the human mandibular condyle. *J. Dent. Res.* **79**, 957–963 (2000).
59. Peters, O. A., Laib, A., Rueggsegger, P. & Barbakow, F. Three-dimensional analysis of root canal geometry by high-resolution computed tomography. *J. Dent. Res.* **79**, 1405–1409 (2000).
60. Sasaki, H. et al. IL-10, but not IL-4, suppresses infection-stimulated bone resorption *in vivo*. *J. Immunol.* **165**, 3626–3630 (2000).
61. Duyck, J. et al. The influence of static and dynamic loading on marginal bone reactions around osseointegrated implants: an animal experimental study. *Clin. Oral Implants Res.* **12**, 207–218 (2001).
62. Zeltinger, J., Sherwood, J. K., Graham, D. A., Müller, R. & Griffith, L. G. Effect of pore size and void fraction on cellular adhesion, proliferation & matrix deposition. *Tissue Eng.* **7**, 557–572 (2001).
63. Lin, A. S., Barrows, T. H., Cartmell, S. H. & Guldberg, R. E. Microarchitectural and mechanical characterization of oriented porous polymer scaffolds. *Biomaterials* **24**, 481–489 (2003).
64. Lutolf, M. P. et al. Repair of bone defects using synthetic mimetics of collagenous extracellular matrices. *Nat. Biotechnol.* **21**, 513–518 (2003).
65. Jones, A. C. et al. Analysis of 3D bone ingrowth into polymer scaffolds via micro-computed tomography imaging. *Biomaterials* **25**, 4947–4954 (2004).
66. Williams, J. M. et al. Bone tissue engineering using polycaprolactone scaffolds fabricated via selective laser sintering. *Biomaterials* **26**, 4817–4827 (2005).
67. Gluer, C. C., Wu, C. Y., Jergas, M., Goldstein, S. A. & Genant, H. K. Three quantitative ultrasound parameters reflect bone structure. *Calcif. Tissue Int.* **55**, 46–52 (1994).

68. Nicholson, P. H. *et al.* Do quantitative ultrasound measurements reflect structure independently of density in human vertebral cancellous bone? *Bone* **23**, 425–431 (1998).
69. Laib, A. & Rüeggsegger, P. Calibration of trabecular bone structure measurements of *in vivo* three-dimensional peripheral quantitative computed tomography with 28-microm-resolution microcomputed tomography. *Bone* **24**, 35–39 (1999).
70. Engelke, K., Graeff, W., Meiss, L., Hahn, M. & Dellng, G. High spatial resolution imaging of bone mineral using computed microtomography. Comparison with microradiography and undecalcified histologic sections. *Invest. Radiol.* **28**, 341–349 (1993).
71. Bonse, U. *et al.* 3D computed X-ray tomography of human cancellous bone at 8 microns spatial and 10(–4) energy resolution. *Bone Miner.* **25**, 25–38 (1994).
72. Salome, M. *et al.* A synchrotron radiation microtomography system for the analysis of trabecular bone samples. *Med. Phys.* **26**, 2194–2204 (1999).
73. Stambanoni, M., Borchert, G., Abela, R. & Rügsegger, P. Nanotomography based on double asymmetrical Bragg diffraction. *Appl. Phys. Lett.* **82**, 2922–2924 (2003).
74. Nuzzo, S. *et al.* Synchrotron radiation microtomography allows the analysis of three-dimensional microarchitecture and degree of mineralization of human iliac crest biopsy specimens: effects of etidronate treatment. *J. Bone Miner. Res.* **17**, 1372–1382 (2002).
75. Borah, B. *et al.* The effect of risedronate on bone mineralization as measured by micro-computed tomography with synchrotron radiation: correlation to histomorphometric indices of turnover. *Bone* **37**, 1–9 (2005).
76. Bousson, V. *et al.* Cortical bone in the human femoral neck: three-dimensional appearance and porosity using synchrotron radiation. *J. Bone Miner. Res.* **19**, 794–801 (2004).
77. Matsumoto, T., Yoshino, M., Uesugi, K. & Tanaka, M. Biphasic change and disuse-mediated regression of canal network structure in cortical bone of growing rats. *Bone* **41**, 239–246 (2007).
78. Schneider, P. *et al.* Ultrastructural properties in cortical bone vary greatly in two inbred strains of mice as assessed by synchrotron light based micro- and nano-CT. *J. Bone Miner. Res.* **22**, 1557–1570 (2007).
79. Weiss, D. *et al.* Computed tomography of cryogenic biological specimens based on X-ray microscopic images. *Ultramicroscopy* **84**, 185–197 (2000).
80. Thurner, P. J. *et al.* Time-lapsed investigation of three-dimensional failure and damage accumulation in trabecular bone using synchrotron light. *Bone* **39**, 289–299 (2006).
81. Larrue, A., Rattner, A., Laroche, N., Vico, L. & Peyrin, F. Feasibility of micro-crack detection in human trabecular bone images from 3D synchrotron microtomography. *Conf. Proc. IEEE Eng. Med. Biol. Soc.* **2007**, 3918–3921 (2007).
82. Koester, K. J., Ager, J. W. 3rd & Ritchie, R. O. The true toughness of human cortical bone measured with realistically short cracks. *Nat. Mater.* **7**, 672–677 (2008).
83. Parfitt, A. M. *et al.* Relationships between surface, volume & thickness of iliac trabecular bone in aging and in osteoporosis. Implications for the microanatomic and cellular mechanisms of bone loss. *J. Clin. Invest.* **72**, 1396–1409 (1983).
84. Hildebrand, T., Laib, A., Müller, R., Dequeker, J. & Rügsegger, P. Direct three-dimensional morphometric analysis of human cancellous bone: microstructural data from spine, femur, iliac crest, and calcaneus. *J. Bone Miner. Res.* **14**, 1167–1174 (1999).
85. Odgaard, A. Three-dimensional methods for quantification of cancellous bone architecture. *Bone* **20**, 315–328 (1997).
86. Hildebrand, T. & Rügsegger, P. Quantification of bone microarchitecture with the structure model index. *Comput. Methods Biomech. Biomed. Engin.* **1**, 15–23 (1997).
87. Whitehouse, W. J. The quantitative morphology of anisotropic trabecular bone. *J. Microsc.* **101**, 153–168 (1974).
88. Odgaard, A. & Gundersen, H. J. Quantification of connectivity in cancellous bone, with special emphasis on 3-D reconstructions. *Bone* **14**, 173–182 (1993).
89. Serra, J. *Image Analysis and Mathematical Morphology* (Academic Press, London, UK, 1982).
90. Gombert, B. R., Saha, P. K. & Wehrli, F. W. Topology-based orientation analysis of trabecular bone networks. *Med. Phys.* **30**, 158–168 (2003).
91. Stauber, M. & Müller, R. Volumetric spatial decomposition of trabecular bone into rods and plates—a new method for local bone morphometry. *Bone* **38**, 475–484 (2006).
92. Stauber, M. & Müller, R. Age-related changes in trabecular bone microstructures: global and local morphometry. *Osteoporos. Int.* **17**, 616–626 (2006).
93. Liu, X. S. *et al.* Complete volumetric decomposition of individual trabecular plates and rods and its morphological correlations with anisotropic elastic moduli in human trabecular bone. *J. Bone Miner. Res.* **23**, 223–235 (2008).
94. Stauber, M., Rapillard, L., van Lenthe, G. H., Zysset, P. & Müller, R. Importance of individual rods and plates in the assessment of bone quality and their contribution to bone stiffness. *J. Bone Miner. Res.* **21**, 586–595 (2006).
95. Cooper, D. M. *et al.* Age-dependent change in the 3D structure of cortical porosity at the human femoral midshaft. *Bone* **40**, 957–965 (2007).
96. Voide, R., van Lenthe, G. H. & Müller, R. Bone morphometry strongly predicts cortical bone stiffness and strength, but not toughness, in inbred mouse models of high and low bone mass. *J. Bone Miner. Res.* **23**, 1194–1203 (2008).
97. Turner, C. H. Bone strength: current concepts. *Ann. NY Acad. Sci.* **1068**, 429–446 (2006).
98. Boivin, G. Y., Chavassieux, P. M., Santora, A. C., Yates, J. & Meunier, P. J. Alendronate increases bone strength by increasing the mean degree of mineralization of bone tissue in osteoporotic women. *Bone* **27**, 687–694 (2000).
99. Roschger, P., Paschalis, E. P., Fratzi, P. & Klaushofer, K. Bone mineralization density distribution in health and disease. *Bone* **42**, 456–466 (2008).
100. Nazarian, A., Snyder, B. D., Zurakowski, D. & Müller, R. Quantitative micro-computed tomography: a non-invasive method to assess equivalent bone mineral density. *Bone* **43**, 302–311 (2008).
101. Kazakia, G. J., Burghardt, A. J., Cheung, S. & Majumdar, S. Assessment of bone tissue mineralization by conventional x-ray microcomputed tomography: comparison with synchrotron radiation microcomputed tomography and ash measurements. *Med. Phys.* **35**, 3170–3179 (2008).
102. Fajardo, R. J. *et al.* Specimen size and porosity can introduce error into microCT-based tissue mineral density measurements. *Bone* **44**, 176–184 (2009).
103. Yang, G. *et al.* The anisotropic Hooke's law for cancellous bone and wood. *J. Elast.* **53**, 125–146 (1998).
104. Müller, R., Hannan, M., Smith, S. Y. & Bauss, F. Intermittent ibandronate preserves bone quality and bone strength in the lumbar spine after 16 months of treatment in the ovariectomized cynomolgus monkey. *J. Bone Miner. Res.* **19**, 1787–1796 (2004).
105. Hodgskinson, R. & Currey, J. D. The effect of variation in structure on the Young's modulus of cancellous bone: a comparison of human and non-human material. *Proc. Inst. Mech. Eng. [H]*. **204**, 115 (1990).
106. Hou, F. J., Lang, S. M., Hoshaw, S. J., Reimann, D. A. & Fyhrie, D. P. Human vertebral body apparent and hard tissue stiffness. *J. Biomech.* **31**, 1009–1015 (1998).
107. Müller, R., Gerber, S. C. & Hayes, W. C. Micro-compression: a novel technique for the nondestructive assessment of local bone failure. *Technol. Health Care* **6**, 433–444 (1998).
108. Nazarian, A. & Müller, R. Time-lapsed microstructural imaging of bone failure behavior. *J. Biomech.* **37**, 55–65 (2004).
109. Müller, R. *et al.* Micromechanical evaluation of bone microstructures under load. In *Developments in X-Ray Tomography III (Proceedings Volume 4503)* (Ed. Bonse, U.) 189–200 (SPIE, San Diego, CA, 2002).
110. Nagaraja, S., Couse, T. L. & Goldberg, R. E. Trabecular bone microdamage and microstructural stresses under uniaxial compression. *J. Biomech.* **38**, 707–716 (2005).
111. Hulme, P. A., Ferguson, S. J. & Boyd, S. K. Determination of vertebral endplate deformation under load using micro-computed tomography. *J. Biomech.* **41**, 78–85 (2008).
112. Thurner, P. J. *et al.* High-speed photography of compressed human trabecular bone correlates whitening to microscopic damage. *Eng. Fract. Mech.* **74**, 1928–1941 (2007).
113. Weiner, S., Traub, W. & Wagner, H. D. Lamellar bone: structure-function relations. *J. Struct. Biol.* **126**, 241–255 (1999).
114. Voide, R. *et al.* Functional microimaging: a hierarchical investigation of bone failure behavior. *J. Jpn. Soc. Bone Morphom.* **18**, 9–21 (2008).
115. Nalla, R. K., Stolken, J. S., Kinney, J. H. & Ritchie, R. O. Fracture in human cortical bone: local fracture criteria and toughening mechanisms. *J. Biomech.* **38**, 1517–1525 (2005).
116. Di Michiel, M. *et al.* Fast microtomography using high energy synchrotron radiation. *Rev. Sci. Instrum.* **76**, 043702 (2005).
117. Meier, M., Vogel, P., Voide, R., Schneider, P. & Müller, R. Investigation of microdamage in murine bone under dynamic load. *J. Biomech.* **41** (Suppl. 1), S76 (2008).

Acknowledgments

The author would like to acknowledge support from the Swiss National Science Foundation. Special thanks to Drs. T. Kohler, T. L. Mueller, P. Schneider, G. H. van Lenthe and R. Voide for generously providing images.